

Deuterium irradiation-induced defect concentrations in tungsten

K Heinola¹, T Ahlgren¹, E Vainonen-Ahlgren², J Likonen²
and J Keinonen¹

¹ Accelerator Laboratory, P O Box 64, FIN-00014 University of Helsinki, Finland

² VTT Processes, Association EURATOM-Tekes, P O Box 1000, FIN-02044 VTT, Finland

E-mail: kalle.heinola@helsinki.fi

Received 10 October 2006

Accepted for publication 7 December 2006

Published 8 March 2007

Online at stacks.iop.org/PhysScr/T128/91

Abstract

Deuterium retention in the implantation-induced defects in polycrystalline tungsten has been studied. Deuterium was implanted with different energies and concentrations of retained D were analysed with secondary ion mass spectrometry and nuclear reaction analysis. Annealings were carried out at four pre-determined temperatures corresponding to four different defect types that can trap deuterium. A quantitative number of each defect type produced by 5, 15 and 30 keV D implantation with a dose of $5.8 \times 10^{16} \text{ cm}^{-2}$ was obtained.

PACS numbers: 25.55.Ci, 61.18.Bn, 61.80.Jh, 66.30.Jt

1. Introduction

In fusion devices, hydrogen escaping the plasma can cause hydrogen build-up in the subsurface region of the first wall materials. Captured hydrogen can be partly released back to the plasma, and at the same time retention in the wall materials also takes place. Retention is affected by several parameters e.g., incoming hydrogen energy, net damage in the material and presence of trapping impurities. The hydrogen recycling will influence the particle balance in the plasma.

Tungsten (W) is a valid candidate as plasma facing material in fusion devices. Its high melting point, good thermal conductivity, and low sputtering yields make it a suitable material to be used in extreme conditions in divertor and baffle areas. Nevertheless, because W is a high-Z material, sputtered W particles cause great plasma power losses and plasma contamination.

Recycling of hydrogen isotopes in tungsten has been studied extensively in the literature [1–7]. In the course of ion implantation, different types of ion trapping defects are formed, namely host material interstitials, vacancies and clusters. In addition to this lattice damage, the host material holds other trapping defects that exist *a priori* implantation, i.e. grain boundaries and impurity atoms working as effective ion trapping sites. Formation of implantation damage is a dynamical process where highly mobile interstitials and almost immobile vacancies interact with each other e.g.,

recombining correlatedly or uncorrelatedly (Frenkel pair recombinations), forming clusters, diffusing to the sample surface or deeper into the bulk. Some part of the implanted ions gets backscattered from the sample surface and the rest penetrates into the sample. In the case of hydrogen implantation into W, the free hydrogen can be trapped at defects, out-diffuse from the bulk to the surface or diffuse deeper into the bulk far beyond the implantation zone because of its low-diffusion activation energy 0.39 eV [8]. During implantation and defect formation recovery processes also take place, where interstitials annihilate with vacancies, react with other interstitials and impurities, or interstitials get detrapped and interstitial clusters are formed. Once implantation is stopped this dynamical defect formation-recovery process gets stabilized and the untrapped ions and interstitials get immobilized by trapping at some defect or simply diffuse out from the bulk. During the annealing of the deuterium (D) implanted W samples, the recorded quadrupole mass-spectrometer (QMS) signal of D₂ can be referred, besides thermal detrapping of D, to certain recovery stages that take place in the sample material and which induce the out-gassing of D₂ molecules.

In the present study, the number and concentration profiles for defects that trap hydrogen were determined. The deuterium implantation energies were chosen to be 5, 15 and 30 keV per D ion in order to make the depth profile measurements for hydrogen traps accurate enough. As will be

seen in section 3, the lowest D concentrations detected in this study were in the limits of secondary ion mass spectrometry (SIMS) and QMS sensitivity. Also the presence of different defect types are explained with different sample recovery stages in the course of annealing.

2. Experimental

2.1. Sample preparation and QMS

The sample material was high purity (99.99%) polycrystalline W sheet (thickness of 1 mm) produced by Plansee AG (Reutte, Austria). The sheet was cut into pieces ($15 \times 10 \text{ mm}^2$) which were mirror-polished with colloidal silica (grain size of $\sim 0.05 \mu\text{m}$). A 3D stylus profilometer (KLA-Tencor P-15 Profiler) was used to measure the surface roughness, which was less than 10 nm root mean square. The samples were pre-annealed at about 1370 K for 2 h *a priori* implantation in order to reduce the grain boundaries within the samples.

Implantation was carried out at room temperature using 10, 30 and 60 keV D_2^+ ions (5, 15 and 30 keV per deuteron, respectively) perpendicular to the surface in a vacuum of $\sim 10^{-8}$ mbar. The implantation dose was $5.8 \times 10^{16} \text{ D cm}^{-2}$. A reference sample for calibrating the D concentrations was prepared by implanting 30 keV D_2^+ ions to a fluence of $7.34 \times 10^{16} \text{ D cm}^{-2}$ into silicon.

Annealing was carried out in a quartz-tube furnace equipped with a QMS. The temperature was measured with a calibrated thermocouple in direct contact with the W surface. During annealing of the sample, the D_2 partial pressure varied between 10^{-13} – 10^{-10} mbar, while the total pressure in the chamber was less than 10^{-7} mbar.

2.2. SIMS and nuclear reaction analysis (NRA)

The D concentration profiles were measured by combining the SIMS and NRA techniques. The benefits of good depth resolution of SIMS and the quantitiveness of the NRA method made it possible to study the D trapping defects produced by the low implantation dose.

The SIMS measurements were done using 5 keV O_2^+ primary ions. The primary ion current was 250 nA and analysed area $290 \times 430 \mu\text{m}$. Crater wall effects were avoided by using a 10% electronic gate and 1 mm optical gate. The pressure inside the analysis chamber was 5×10^{-8} mbar during the analysis. The depth of the craters was measured by a profilometer (Dektak 3030ST). The uncertainty of the crater depth was estimated to be 10%. W and D were profiled using W^+ ($m/e = 184$) and WD^+ ($m/e = 188$) signals [9].

The NRA measurements were carried out using the $\text{D}({}^3\text{He}, \text{p}){}^4\text{He}$ nuclear reaction which has a relatively broad differential cross-section peak of $\sim 60 \text{ mb sr}^{-1}$ near 640 keV ${}^3\text{He}$ energy [10, 11]. At ${}^3\text{He}$ energies below 1.2 MeV the differential cross-section is angle independent [11–13]. A 700 keV ${}^3\text{He}^{2+}$, 2.0 mm in diameter collimated beam at 40° incident angle from the sample normal was used. A $4 \mu\text{m}$ Al foil was put in front of the 1500 μm thick wide-angle silicon detector to stop the backscattered ${}^3\text{He}$. The solid angle of the detector was 0.19 sr and was placed at 60° to the incident beam. This geometry provides the reaction angle

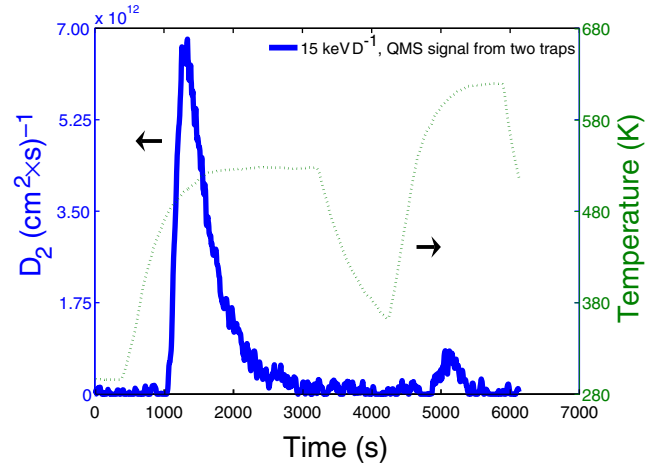


Figure 1. QMS spectra showing two D_2 peaks from 15 keV D^{-1} implanted sample. The majority of the retained D is released in the first annealing 520 K (left-hand side peak with maximum height at $\sim 6.8 \times 10^{12} \text{ D}_2 (\text{cm}^2 \times \text{s})^{-1}$). The second peak is present at the following annealing stage at 610 K (right-hand side peak with maximum at $\sim 8.7 \times 10^{11} \text{ D}_2 (\text{cm}^2 \times \text{s})^{-1}$). Peaks present two different defect types which are fully emptied of D in the course of annealing.

120° . Protons from the $\text{D}({}^3\text{He}, \text{p}){}^4\text{He}$ reaction with 13.7 MeV energy were collected for the analysis. The wide aperture of the detector $\pm 12^\circ$ caused a $\pm 250 \text{ keV}$ geometrical straggling to the detected protons. The Al foil caused a minor additional energy straggling of about 4.9 keV. It is worth emphasizing that the large solid angle of the detector and the energy spread did not have any effect on the analysis of the NRA spectra since only the total number of counts in the proton peak area were of interest.

The conversion of yield to D concentration of the SIMS depth profiles were done using the SIMNRA computer program [14]. For each sample, the SIMS D depth distribution was given as input to the program and the height of the D concentration was then varied until the SIMNRA simulated proton yield matched with the experimental NRA spectra. The ${}^3\text{He}^{2+}$ ion charge was calibrated using a D implanted silicon standard together with a beam chopper system.

3. Results

3.1. QMS

The D implanted W samples were annealed at different temperatures and the D_2 molecules desorbed from the W surface were recorded *in-situ* with QMS. The four annealing temperatures between 520 and 875 K were chosen according to our earlier study [15]. After implantation at room temperature only trapped D ions are present because the free highly mobile D has diffused away from the implanted region. The four temperatures refer to different D trapping defect types or a defect recovery stages in W. These defects have different binding energies that can be defined as the energy difference between a trapped and a solute D atom. Section 4 discusses the origin of these defect types. Annealing was performed as follows. Annealing temperature increased until the predetermined temperature is reached. Then the

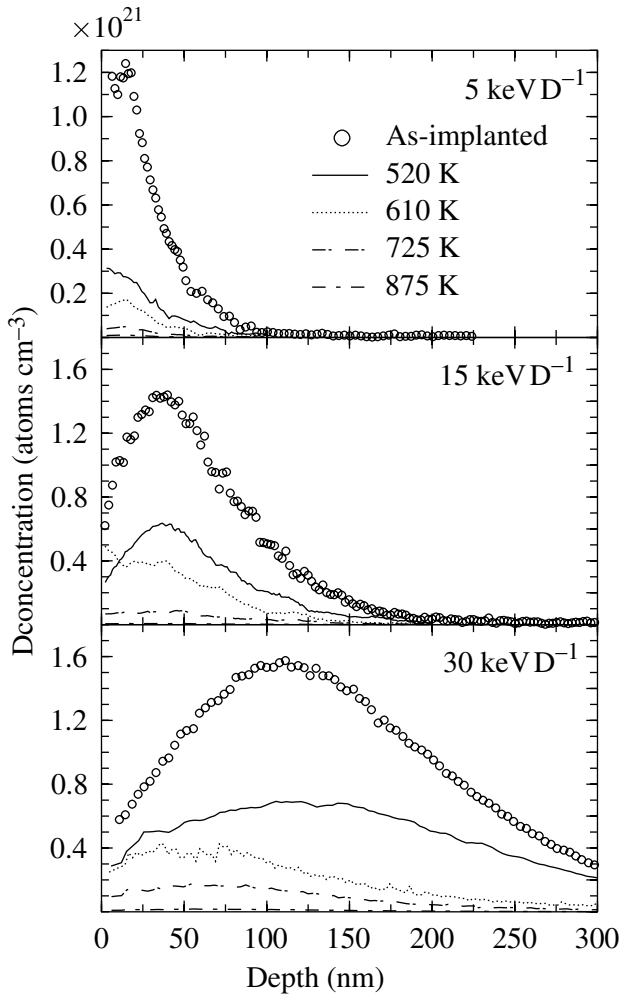


Figure 2. D depth profiles measured by SIMS. Increasing implantation energy causes deeper penetration of D into W sample, and growth of the concentrations of D trapping defects. Annealing of the samples reveals the retained D in each defect type. See section 4 for details.

temperature was kept constant until QMS signal monitoring the D_2 molecule release from the sample dropped to null, indicating that all D atoms have been removed from the present trap. This is clearly seen in figure 1 where the QMS signal reaches its maximum at a specific trap and then drops to zero as all the D have out-diffused from this trap. To empty the next trap of D, the annealing procedure is repeated with a corresponding temperature. This can be seen as the second peak in the QMS spectra in figure 1. Similar annealing procedures for all the traps were carried out for 5, 15 and 30 keV D^{-1} implanted samples. Recorded QMS signals were calibrated according to differences in retained D concentrations in sequentially annealed W samples. The QMS data was checked with a calibrated D_2 leak bottle and the deviation from NRA calibration was less than 7% [15].

3.2. SIMS and NRA

SIMS and NRA techniques were used to obtain accurate concentration profiles for the different D traps, i.e., the concentration profiles of retained D in the samples. Figure 2

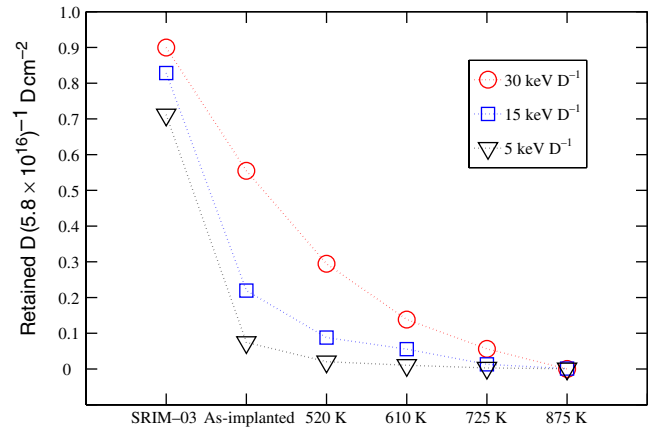


Figure 3. Retained D concentration relative to implantation dose $5.8 \times 10^{16} D cm^{-2}$ presented as a function of annealing temperature. SRIM-03 results (including backscattering) are shown as a reference to the measured as-implanted D concentration. Annealing of the W samples decreases retained D concentration gradually via different recovery mechanisms (see text for details).

presents the D depth profiles of each sample measured with SIMS and normalized with NRA.

The areas for the collected proton NRA spectra were over 1000 counts in most of the samples, giving a statistical uncertainty of about 3% for the profile areas. Only two samples, with integrated D areas of less than $7 \times 10^{13} D cm^{-2}$ (see samples 875 K, 5 and 15 keV D^{-1} in table 1), had a collected proton count of about 100 giving a statistical uncertainty $\sim 10\%$. The collected rotor counts to normalize the collected charge for each measurement exceeded 50 000 counts, adding no significant error to the measurements. Some uncertainty is present concerning the accuracy of the 3He stopping powers in W and Si. This systematic error is the same for all W samples, and the ratios of the concentration profiles should be quite unaffected by the possible error in the stopping power.

As is clearly seen in figure 2, the D concentration peak is located deeper in the sample with increasing implantation energy. SRIM simulations [16] provide a D profile where the maximum of the concentration is located about 80% deeper than that obtained in the experiment for every implantation energy. This discrepancy is explained by the fact that the implanted D does not halt in the implantation region, but diffuses rapidly away from it or gets trapped by implantation-induced damage. This is qualitatively proven by the fact that the SRIM-simulated vacancy profiles, indicating where the implantation-induced damage mostly forms, coincide well with the experimental as-implanted D profiles.

In figure 2 it is also shown that different D implantation energies create varying amounts of defects at various depths. As the incoming D energy increases, the number of trapped D increases and the maximum of the D profiles moves deeper into the sample. The amount of D retained in each defect type is presented in table 1. The amount of retained D in the as-implanted W was found to be 4.3×10^{15} , 1.3×10^{16} and $3.2 \times 10^{16} D cm^{-2}$ for implantation energies 5, 15 and 30 keV, respectively. Fractions of the retained D as a function of temperature for D implantation energies 5, 15 and 30 keV are presented in figure 3.

Table 1. Retained D concentration after 30, 15 and 5 keV D⁻¹ implantation with dose of 5.8×10^{16} D cm⁻². In the table are presented the SRIM simulated results which include backscattering and the SIMS experimental results from as-implanted and annealed W samples (in units of D cm⁻²)

	30 keV	15 keV	5 keV
SRIM	5.2×10^{16}	4.8×10^{16}	4.1×10^{16}
As-implanted	3.2×10^{16}	1.3×10^{16}	4.3×10^{15}
520 K	1.7×10^{16}	5.1×10^{15}	1.2×10^{15}
610 K	8.0×10^{15}	3.2×10^{15}	6.1×10^{14}
725 K	3.3×10^{15}	7.6×10^{14}	1.7×10^{14}
875 K	3.2×10^{14}	6.5×10^{13}	4.0×10^{13}

The quantitative number of each defect type can be obtained from the retained amount of D (table 1). For 30 keV D⁻¹ implantation the number of defects are 1.5×10^{16} , 9.1×10^{15} , 4.8×10^{15} and 3.0×10^{15} cm⁻² for trapping sites with increasing release temperature, respectively, if each trap is occupied by single D. The same numbers for 15 keV D⁻¹ are respectively 7.9×10^{15} , 1.9×10^{15} , 2.4×10^{15} and 7.0×10^{15} cm⁻² and for 5 keV D⁻¹ 3.1×10^{15} , 5.9×10^{14} , 4.4×10^{14} and 1.3×10^{13} cm⁻².

4. Discussion and conclusions

According to recovery studies conducted by Keys *et al* [17] and Anand *et al* [18], our D₂ QMS signals from annealings at 520, 610 and 725 K refer to recovery stage III of the W sample, which involve self-interstitial migration and divacancy and/or impurity migration and/or interstitials which have escaped from shallow traps. The migrating self-interstitials originate from interstitial clusters, dislocations and grain boundaries.

The amount of retained D after implantation decreases rapidly with decreasing implantation energy. This can be evidently seen in table 1 and figure 3, where the retained amount of D compared to implantation fluence decreases from 55 to 22 and further to 7% with decreasing implantation energy 30, 15 and 5 keV D⁻¹, respectively. A part of this decrease is due to increased D backscattering with decreasing implantation energy: 10, 17 and 29% backscattered D with 30, 15 and 5 keV D⁻¹, respectively. However, the main reason for the rapid decrease in the retained D is the increase of the recombination rate of implantation-induced self-interstitials and vacancies with decreasing implantation energy, resulting in a decrease in the number of defects to which D can be trapped.

Figure 3 presents the amount of D still trapped after each annealing stage. We can observe that the major part of the as-implanted D is lost in the first annealing at about 525 K. The part lost from the as-implanted amount increases from 47 to 61 and further to 72% for decreasing implantation energies 30, 15 and 5 keV D⁻¹, respectively. The reason for this can be found by looking more closely at what happens during implantation; a part of the implantation-induced mobile self-interstitials annihilate with vacancies trapped in grain boundaries, the rest of them form interstitial clusters or diffuse away from the implantation zone. At lower implantation energies these processes happen closer to the surface leading

to a high number of self-interstitials being lost to the surface sink. This means that at lower implantation energies, the fraction of interstitials to vacancies is smaller than at higher energies. This conclusion, that the first annealing stage could be partly assigned to the D detrapping from vacancies or vacancy clusters, explains the trend of increasing D lost in the first annealing. This is also supported by the study of Nordlander *et al* [19], where the binding energy of single D to a W vacancy was calculated to be 1.15 eV, which agrees well with the calculated value of our first annealing stage.

The other types of defects at recovery stage III, seen at 610 and 725 K annealings, are then connected with the mobilization of self-interstitials e.g., detrapping from interstitial clusters [17, 18]. The final loss of D during the last annealing temperature 875 K could be assigned to recovery stage IV where vacancies become mobile [17, 20]. At this temperature, the recovery studies indicate that almost all implantation-induced defects are removed [17, 18]. The about hundredth part D left in the implantation zone after 875 K annealing is probably D atoms chemisorbed on inner walls of intrinsic cavities localized at grain boundaries [21].

We have shown that retained D decreases in at least four separate annealing stages in W. The amount of D is seen to decrease in all annealing stages when D implantation energy decreases. This decrease can be explained by the increasing fraction of vacancies to self-interstitials with decreasing implantation energy. However, to identify the thermal development of defects and hydrogen in W unambiguously, more accurate studies and first principle calculations are still needed.

Acknowledgments

This study was supported by the Association EURATOM-Tekes.

References

- [1] Anderl R A, Holland D F, Longhurst G R, Pawedko R J, Trybus C L and Sellers C H 1992 *Fusion Technol.* **21** 745
- [2] Haasz A A, Davis J W, Poon M and Macalay-Combe R G 1998 *J. Nucl. Mater.* **258–63** 889
- [3] Causey R, Wilson K, Venhaus T and Wampler W R 1999 *J. Nucl. Mater.* **266–69** 467
- [4] Haasz A A, Poon M and Davis J W J 1999 *Nucl. Mater.* **266–69** 520
- [5] Haasz A A, Poon M, Macalay-Combe R G and Davis J W 2001 *J. Nucl. Mater.* **290–93** 85
- [6] Alimov V Kh, Ertl K, Roth J and Schmidt K 2001 *Phys. Scr. T* **94** 34
- [7] Alimov V Kh 2004 *Phys. Scr. T* **108** 46
- [8] Frauenfelder R 1969 *J. Vac. Sci. Technol.* **6** 388
- [9] Tokunaga K, Takayama M, Muroga T and Yoshida N 1995 *J. Nucl. Mater.* **220–22** 800
- [10] Kunz W E 1955 *Phys. Rev.* **97** 456
- [11] Möller W and Besenbacher F 1980 *Nucl. Instrum. Methods* **168** 111
- [12] Yarnell J L, Lovberg R H and Stratton W R 1953 *Phys. Rev.* **90** 292
- [13] Bonner T W, Conner J P and Lillie A B 1952 *Phys. Rev.* **88** 456
- [14] Mayer M 1997 *SIMNRA's User's Guide, Tech. Rep. IPP 9/113* (Garching: Max-Planck-Institut für Plasmaphysik)

- [15] Ahlgren T, Heinola K, Vainonen-Ahlgren E, Likonen J and Keinonen J 2006 *Nucl. Instrum. Methods B* **249** 436
- [16] Ziegler J F SRIM-03 software package. Online at: <http://www.srim.org>
- [17] Keys L K, Smith J P and Moteff J 1968 *Phys. Rev.* **176** 851
- [18] Anand M S, Pande B M and Agarwala R P 1978 *Radiat. Effects* **39** 149
- [19] Nordlander P, Nørskov J K and Besenbacher F 1986 *J. Phys. F: Met. Phys.* **16** 1161
- [20] Rasch K D, Siegel R W and Schultz H 1979 *Phil. Mag.* A **41** 91
- [21] Alimov V Kh and Roth J 2007 *Phys. Ser. T* **128** 6